Hindawi
Geofluids
Volume 2019, Article ID 8053579, 14 pages
https://doi.org/10.1155/2019/8053579

Research Article

Volcanogenic CO_2 Degassing in the Songliao Continental Rift System, NE China

Wenbin Zhao,[1,2,3] Zhengfu Guo,[1,2,3] Ming Lei,[1,2,3] Maoliang Zhang,[1,2,3] Lin Ma,[1,2,3] Danielle Fortin,[4] and Guodong Zheng[5,6]

[1]*Key Laboratory of Cenozoic Geology and Environment, Institute of Geology and Geophysics, Chinese Academy of Sciences, Beijing 100029, China*
[2]*CAS Center for Excellence in Life and Paleoenvironment, Beijing 100044, China*
[3]*College of Earth and Planetary Sciences, University of Chinese Academy of Sciences, Beijing 100049, China*
[4]*Department of Earth and Environmental Sciences, University of Ottawa, Ottawa, Ontario, Canada K1N 6N5*
[5]*Northwest Institute of Eco-Environment and Resources, Chinese Academy of Sciences, Lanzhou 730000, China*
[6]*Key Laboratory of Petroleum Resources, Gansu Province, Lanzhou 730000, China*

Correspondence should be addressed to Zhengfu Guo; zfguo@mail.iggcas.ac.cn

Received 26 January 2019; Revised 14 May 2019; Accepted 17 June 2019; Published 19 August 2019

Academic Editor: Giovanni Martinelli

The Wudalianchi monogenetic volcanic field (WMVF) is located in the Songliao basin within a major continental rift system in NE China. Bubbling springs and diffuse degassing from soils are typical features of the WMVF. Chemical compositions and C-He isotope analyses revealed that the cold spring gases might originate from the enriched upper mantle (EM), which resulted from the mixing between slab materials (subducted organic sediments and carbonates) in the mantle transition zone (MTZ) and the ambient depleted mantle. These EM-derived volatiles experienced variable degrees of crustal input, including both continental organic metasediments and crustal carbonates during their ascending path to the surface. The estimated results of the degassing CO_2 fluxes, combined with previous geophysical evidence, suggest that the CO_2 degassing activities become weaker from early to late in Quaternary.

1. Introduction

Continental rift systems, together with the related intraplate volcanism, have been regarded as a possible trigger of deep-derived CO_2 degassing into the atmosphere and long-term climate change [1–6]. Positive spatial correlation between CO_2 discharges and the extensional tectonic regimes confirms that the continental rift systems are critical pathways for deep carbon degassing from the Earth's interior to the exosphere [6]. Research on continental rift lengths and paleoatmospheric CO_2 concentrations over the last 200 million years also indicates that continental fragmentation may control the atmospheric CO_2 levels via massive CO_2 degassing in rift systems [4]. Intraplate volcanism along continental rift systems is primarily derived from the metasomatized mantle [7]. Under these conditions, the reduction of the peridotite solidus due to the presence of volatiles allows for partial melting of the upper mantle at depth and thus for the release of large amounts of CO_2 into the atmosphere via extensive volcanism [4, 5, 8, 9].

The Songliao basin in NE China has experienced long-term extension-induced continental rifting since the Late Mesozoic as indicated by many intraplate volcanoes (Figure 1(a)) [10]. Based on both petrogenesis and geophysical evidences, these Cenozoic volcanic activities have been considered to be linked to the stagnant Pacific slab materials in the mantle transition zone (MTZ) [11–15]. However, the origin and evolution of magma degassing in the continental rift system involving the deep subduction of oceanic slab are poorly understood [16, 17]. Located at the northern margin of the Songliao continental rift system in East Asia (Figure 1(a)), the Wudalianchi monogenetic volcanic field

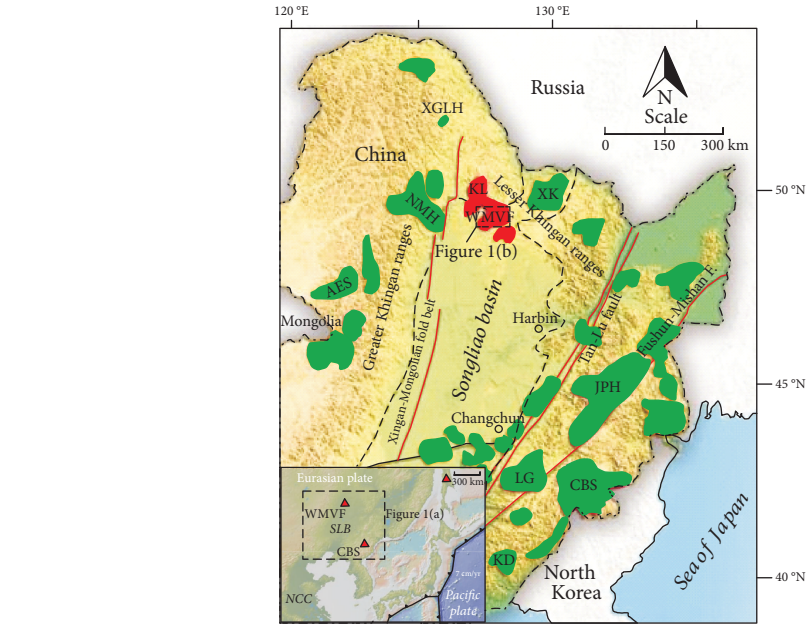

(a)

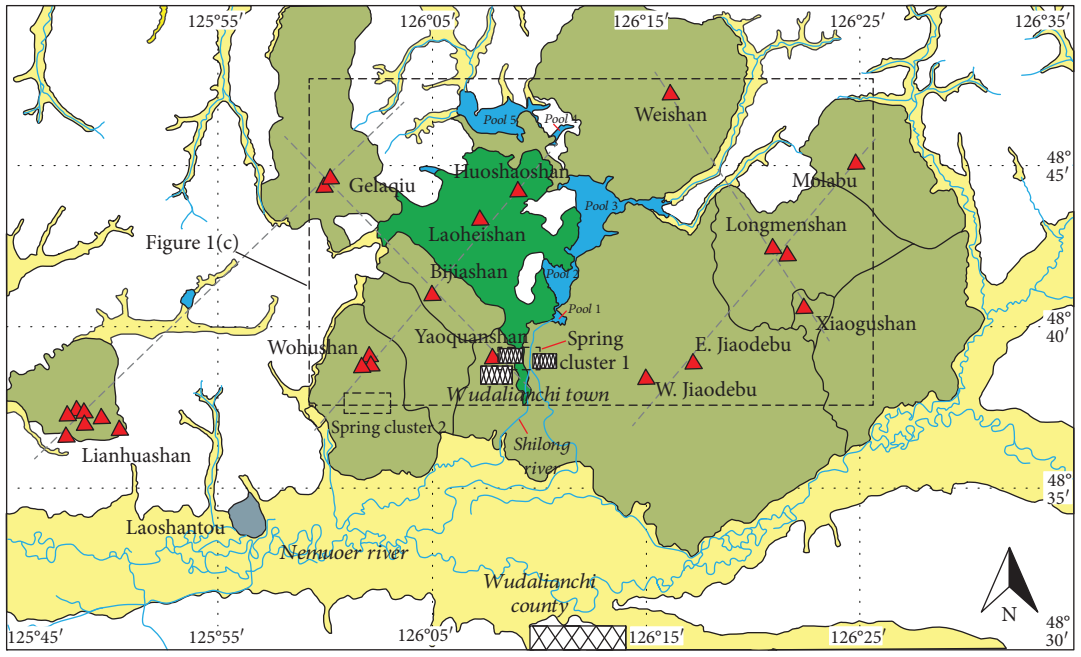

Figure column for Figure 1(b)

- Holocene volcanic rock
- Quaternary fluvial deposit
- Rivers and lakes
- Early Pleistocene volcanic rock
- Monogenetic volcanoes
- Middle and Late Pleistocene volcanic rock
- Speculated faults

(b)

Figure 1: Continued.

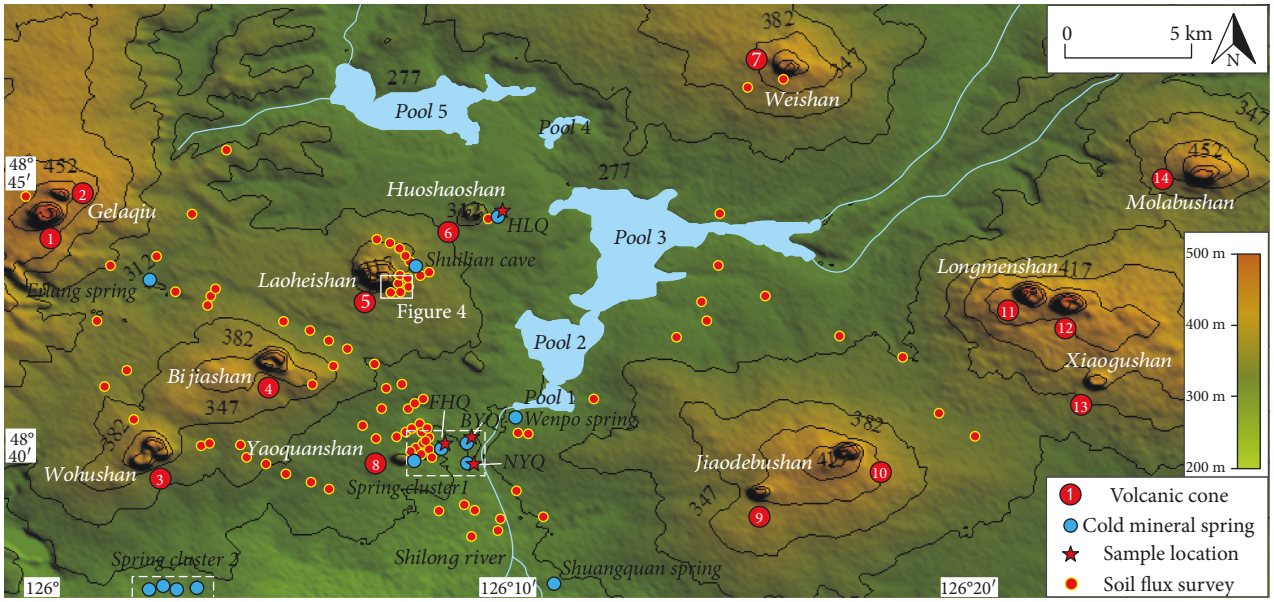

(c)

Figure 1: (a) Geological and tectonic map showing the locations of major faults and Cenozoic basaltic volcanic fields in NE China (modified from Liu et al. [10]). The inset shows the location of Eastern China. Abbreviations of Cenozoic volcanic fields in NE China are as follows: WMVF: Wudalianchi monogenetic volcanic field; XK: Xunke; KL: Keluo; NMH: Nuominhe; XGLH: Xiaogulihe; AES: Aershan; JPH: Jingpohu; LG: Longgang; CBS: Changbaishan; KD: Kuandian; SLB: Songliao basin; NCC: North China craton. (b) Geological map of WMVF (modified from Zhao et al. [23]). (c) Geomorphologic map showing the location of monogenetic volcanoes and cold springs in WMVF. Red dots represent the location of the soil CO_2 flux survey, and the stars represent the sample locations.

(WMVF) is characterized by extensive CO_2 degassing, i.e., cold bubbling springs, diffused CO_2 emissions from soils, and volcanogenic fault systems (Figure 1(b)). CO_2 is supposed to be of mainly magmatic origin, but the mechanisms of deep CO_2 formation are still debated. Some authors [18–21] indicated a binary mixing between the depleted mantle- and upper crust-derived volatiles. Other authors [22] hypothesized partial melting of a subcontinental lithospheric mantle (SCLM) metasomatized by ancient fluids.

In this paper, we report the first soil CO_2 flux measurements in the WMVF. Additionally, new data on the chemical and C-He isotopic composition of gases associated with four cold springs located in the area are presented and used to gain insights into the mechanisms responsible for CO_2 formation at depth.

2. Geological Setting

The Wudalianchi monogenetic volcanic field (WMVF) is an active K-rich volcanic region located in a continental rift system in NE China (Figure 1(a)). Its latest eruption dates back to 1721 AD (e.g., Laoheishan and Huoshaoshan volcanoes, Figures 1(b) and 1(c)) [23, 24]. The WMVF basement consists of Archean granites, Mesozoic andesite, and granite intrusions [25]. Limestones and marine carbonate sediments have been present in outcrops in the ambient Songliao basin since the Mesozoic age [26, 27]. During the Cenozoic period, dispersed calc-alkaline, tholeiitic, and alkali basaltic rocks were formed in Northeastern China [10], which constitute the eastern part of the Asian tectono-magmatic province that extends from Lake Baikal, Siberia, to Eastern China [28].

Cenozoic volcanic activity has formed 800 km^2 of lava flows, which includes the middle Pleistocene to Holocene volcanic activity in WMVF (Figure 1(b)) [23, 24]. These fissure-central-type eruptions are controlled by NE- to NNW-striking fractures or deep faults [23, 29], which are linked to the continental rift systems in East Asia [30, 31]. Deep buried faults provided potential rising channels for the magma [23], which finally led to the unique volcanic landscapes seen nowadays in WMVF [24], such as linear rows of scoria cones (Figures 1(b) and 1(c)), dominant tectonic weakness direction enlarged by erosion (e.g., Huoshaoshan volcanic cone, Figure 2(e)), and overlapping scoria cones (e.g., Wohushan volcanic cone, Figure 1(c)). All of these features were used in the past to locate feeding fissures beneath the monogenetic volcanoes in continental rift systems [32].

Seismic tomography studies have shown the presence of a magma reservoir under the Weishan volcano in WMVF (Figures 1(b) and 1(c)), which is considered as evidence for partial melting in a shallow magma chamber at 7~13 km depth [33]. Surface manifestation of such activity is mainly expressed as cold-mineral bubbling springs with high p_{CO2} and low water temperature (generally between 4 and 7°C), prevalently distributed on the flanks or at the margin of the active volcanic cones (Figure 1(c)) [18, 21], and located roughly at the same elevation (about 300 to 320 m.a.s.l., Figure 1(c)). The Hualin spring (HLQ) is located at the eastern slope of the Huoshaoshan volcanic cone (Figures 1(c)

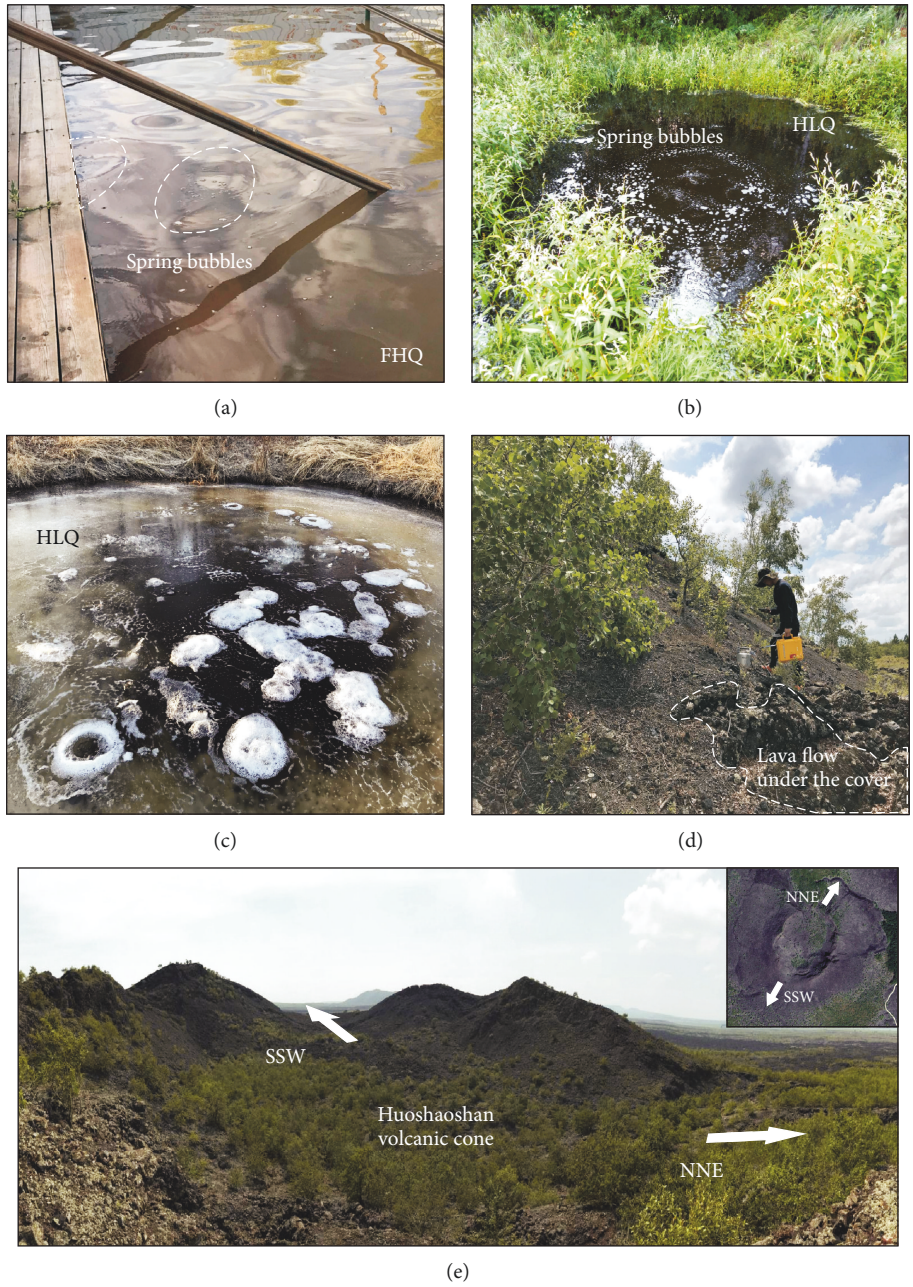

Figure 2: Photos showing the Fanhua spring (a), Hualin spring in August 2017 (b) and April 2019 (c), basaltic lava flow under the thin pumiceous deposits beside the Laoheishan volcanic cone (d), and dominant tectonic weakness direction enlarged by erosion in the Huoshaoshan volcanic cone (e).

and 2(b)) and shows the highest water temperature (24°C) in the WMVF. The North, South, and Fanhua cold springs are located east of the Yaoquanshan volcano and west of the Shilong river (Figure 1(c)) and are characterized by water temperatures lower than 10°C.

3. Sampling and Analytical Methods

3.1. Soil CO_2 Flux Measurements. Soil CO_2 fluxes were measured *in situ* using soil diffuse gas flux meters based on the accumulation chamber method (Figure 2(d)), which was firstly reported by Chiodini et al. [34]. The edge of the inverted cylindrical chamber was sealed with damp soil to diminish air contamination of the soil gases in the chamber [35]. The measurement sites were located near the main volcano-structural features of the region and preferentially placed on uncovered ground to minimize the influence of the vegetation on the measured fluxes (Figure 1(c)). The temperature was measured *in situ* at a depth of 10 cm, and the location was recorded (measured with a Garmin GPSMAP 60SCx) at each measurement point (see details in Supplementary Material). 92 measurement points were made during stable suitable weather and similar atmospheric conditions in August and September 2017. In order to compare

the CO_2 emission rate of the new erupted region with that of the whole WMVF, additional 38 points were considered on the southeastern slope of the Laoheishan volcanic cone (Figures 1(c) and 2(d)), whose last activity occurred about 300 years ago.

3.2. Spring Gas Sampling and Composition Analysis. Gas samples from four cold bubbling springs (Figures 1(c) and 2) were collected by means of the drainage method using lead-bearing glass bottles [16]. The temperature of the spring water was measured *in situ* using a portable thermometer. Chemical and isotopic compositions of the gas samples were measured in the Key Laboratory of Petroleum Resources Research, Institute of Geology and Geophysics, Chinese Academy of Sciences (IGGCAS), Lanzhou, China. The chemical composition of the gas samples was determined using a MAT 271 mass spectrometer. The $\delta^{13}C_{CO2}$ was analyzed with a Delta Plus XP mass spectrometer. All samples were analyzed for the helium isotope composition ($^3He/^4He$) using a Noblesse noble gas mass spectrometer. Detailed analytical procedures are described in Luo et al. [36] and Zhang et al. [37].

4. Results

4.1. Degassing Flux of Soil CO_2. We obtained a broad range of soil CO_2 fluxes (1.1 to 161.5 $g\,m^{-2}\,d^{-1}$) and soil temperatures (18.1°C to 33.3°C; Supplementary Table S1), which demonstrate high variability of soil CO_2 emissions in WMVF. In the log probability plot (Figure 3(a)), our analytical data could be basically divided into the following three groups by two inflection points on the skewed curve [38]: less than 5 $g\,m^{-2}\,d^{-1}$ (Group A), 5-60 $g\,m^{-2}\,d^{-1}$ (Group B), and more than 60 $g\,m^{-2}\,d^{-1}$ (Group C), characterized by average soil CO_2 flux values of 3.5 $g\,m^{-2}\,d^{-1}$, 17.6 $g\,m^{-2}\,d^{-1}$, and 92.1 $g\,m^{-2}\,d^{-1}$, respectively (Figure 3(a)). These groups may represent different sources of soil CO_2 based on Chiodini et al. [39]: (i) biological source with low soil CO_2 flux (e.g., soil respiration or pedochemical process, Group A) and (ii) geological source with high soil CO_2 flux (e.g., magmatic or hydrothermal related carbon degassing, Group C). In particular, Group B with intermediate soil CO_2 fluxes may represent the mixture of biological and geological sources (Figure 3(a)). The average soil CO_2 flux of the whole WMVF was calculated using the weighted mean method, which is 18.7 $g\,m^{-2}\,d^{-1}$. Using the same statistical method, an average soil CO_2 flux of 11.8 $g\,m^{-2}\,d^{-1}$ was obtained for the SE slope of the Laoheishan volcanic cone (Figure 3(b)).

Caracausi et al. [40] proposed that size-normalized CO_2 fluxes inversely correlate with the ages from the last eruptions, which means that active outgassing of volatiles from magmatic bodies would occur for a long time after the last volcanic activity. However, the average soil CO_2 flux in the SE slope of the Laoheishan volcanic cone, which experienced the latest eruption, is lower than that in the whole WMVF (Figure 3). Considering the dispersed cold springs, and the decoupling of soil temperatures and CO_2 fluxes (with a correlation coefficient of 0.0714) in WMVF, we suggest that the resulting weak degassing is due to the solidification and/or cooling down of the underlying magma body beneath the Laoheishan in about 300 years. Our proposal is in good agreement with crustal electric conductivity studies that a rivet-shaped block with high resistivity, which was considered as the result of solidified magma chamber, is distributed beneath the Laoheishan-Huoshaoshan volcanic chain (Figure 1) [41].

In this study, 50 sequential Gaussian simulations were performed over a grid of 108001 square cells (1 × 1 m) covering an area of 0.11 km^2 in the southeastern slope of the Laoheishan volcano (Figure 4). Total CO_2 output in the selected area of the Laoheishan volcano (ca. 0.11 km^2) is 536.3 t/yr (σ = 43.2 t/d), which is a preliminary survey or first-order estimation of diffusive CO_2 degassing in WMVF.

4.2. Chemical and C-He Isotopic Compositions of Cold Spring Gases. The chemical and C-He isotopic compositions of gases from the WMVF cold springs are listed in Table 1. Our analytical results are in excellent agreement with previous studies (Supplementary Table S3) [18–22], which suggest no distinct changes in chemical and isotopic compositions of the spring gases during the last 20 years.

4.2.1. Chemical Composition. Our results show that most of the gas samples from the Wudalianchi cold springs are characterized by high CO_2 content (higher than 90%) and low O_2 content (lower than 1.29%) and N_2 content (3.2%-8.7%) (Table 1), with the exception of the samples from the Fanhua spring (FHQ17 and FHQ18), which are characterized by low CO_2 content (76.7%-80.2%) and relatively high O_2 (~3.66%) and N_2 content (15.8%-22.6%). N_2/Ar ratios of the WMVF samples in this study range from 27 to 75, suggesting an interaction between helium-rich components, air-saturated water (ASW, $N_2/Ar \approx 40$, temperature dependent), and air ($N_2/Ar = 83.6$) [44, 45], as shown by the linear trend from the high He/Ar to ASW and air endpoints (Figure 5(a)). $CO_2/^3He$ ratios ($(0.1\text{-}29.5) \times 10^9$; Table 1 and Figure 6) were calculated using CO_2/He and $^3He/^4He$ ratios, which overlap those of typical arc-related volatiles ($(4.5\text{-}29) \times 10^9$, [46]) and depleted mantle (1.5×10^9, [46]), indicating CO_2 addition and/or loss during volatile ascending processes (Figure 5(b)).

4.2.2. C-He Isotopic Compositions. The isotopic composition of carbon and helium has been successfully used to quantify the carbonate vs. sediment contribution from subducted slab material recycling [46] and the mantle vs. crustal contribution [44], respectively, in hydrothermal and volcanic gases worldwide.

The $\delta^{13}C\text{-}CO_2$ values of the spring gas samples from the WMVF fall between −7.3‰ and −2.5‰ (versus VPDB, Table 1), overlapping with the compositional fields reported for arc-related volatiles (−9.1‰ to −1.3‰, [46]). Some samples show relatively heavier carbon isotope compositions when compared to upper mantle values (-6.5 ± 2.5‰, [46]), suggesting a possible contribution from inorganic carbon-rich components (carbonate rocks, 0 ± 2‰, [53]).

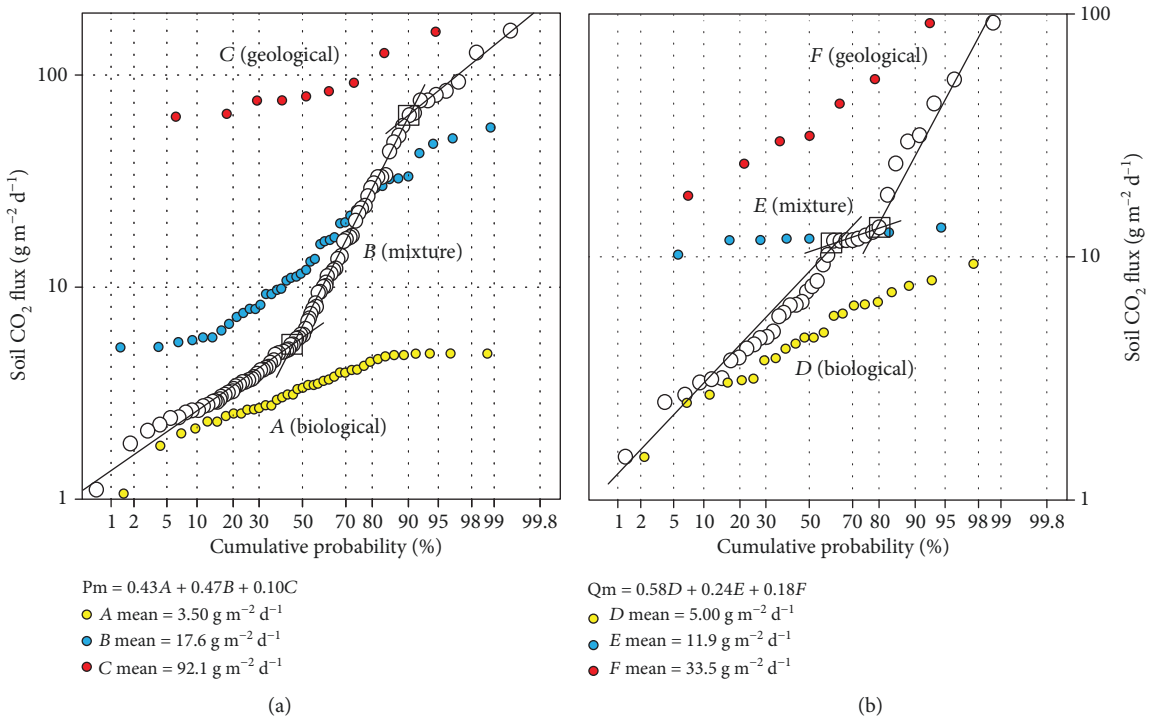

FIGURE 3: Cumulative probability plot of calculated soil CO_2 fluxes in the whole WMVF (a) and SE slope of the Laoheishan volcanic cone (b). Black solid lines represent the partition components of Groups *A*, *B*, and *C* and *D*, *E*, and *F*.

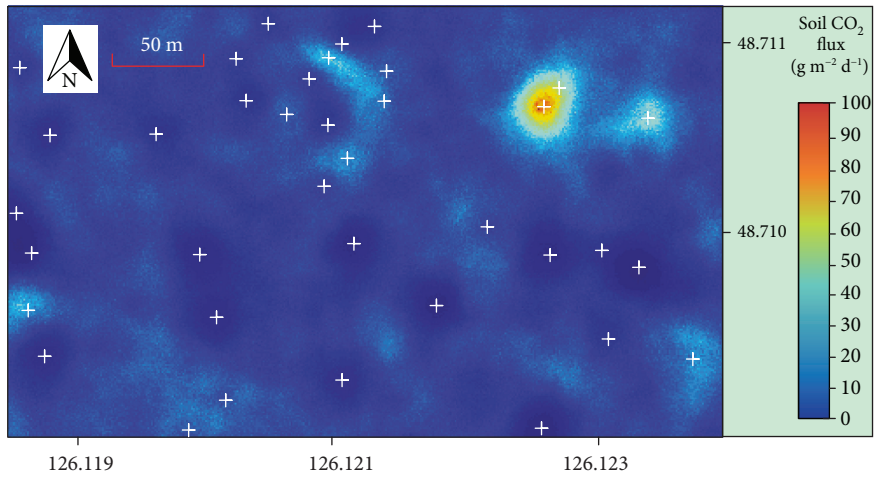

FIGURE 4: CO_2 flux map in the SE slope of the Laoheishan volcanic cone obtained by sequential Gaussian simulations.

Measured $^3He/^4He$ ratios (R_M) of the WMVF gas samples range between $2.26R_A$ and $3.18R_A$ (Table 1), suggesting an obvious contribution from the mantle-derived ^3He (Figures 5–7). Such intermediate helium ratios are lower than those of both the depleted MORB-source mantle (DMM, $8 \pm 1R_A$, [52]) and the subcontinental lithospheric mantle (SCLM, $^3He/^4He = 6.1 \pm 0.9R_A$, [50]), which point to a mixed origin of volatiles from the upper mantle and an end member with high radiogenic ^4He (e.g., crustal materials, $0.02R_A$, [42]) (Table 2 and Figure 7). As the *X* values are high (>150) for all the samples of this study (Table 1), there is little difference between measured (R_M/R_A) and air-corrected (R_C/R_A) helium ratios (Table 1), which indicates little influence from air contamination. Gas samples from the Fanhua spring show higher $^4He/^{20}Ne$ (145-359) and He/Ar ratios (0.28-0.43) (Table 1) than those of the air ($^4He/^{20}Ne = 0.32$, [42]; He/Ar = 0.0005, [54]), which indicate that the high N_2 and low CO_2 contents do not result from the air contamination in the Fanhua spring gases.

5. Discussion

5.1. Carbon Provenance of Volatiles in WMVF. Zhang et al. [16] proposed that the upper mantle (DMM) and slab-

Table 1: Chemical and C-He isotopic compositions of the spring gases in the WMVF.

Sample no.	T (°C)	N_2 (%)	O_2 (%)	Ar (%)	CO_2 (%)	CH_4 (%)	He (ppm)	He/Ar	N_2/Ar	$^4He/^{20}Ne$	R_M/R_A	X	R_C/R_A	$\delta^{13}C$ (‰)	$CO_2/^3He$ ($\times 10^9$)
NYQ17	9.2	8.0	0.35	0.16	91.1	0.07	129	0.08	50	182	2.64	713	2.64	−7.2	1.9
NYQ18	7.7	8.7	0.55	0.18	90.5	0.14	278	0.15	49	153	3.10	597	3.10	−5.6	0.8
BYQ17	7.8	3.4	0.32	0.06	95.8	0.10	379	0.64	58	685	2.26	2675	2.26	−7.3	0.8
BYQ18	6.5	3.2	0.25	0.07	96.5	0.38	18	0.03	46	40	3.16	155	3.17	−6.0	12.1
HLQ17	19.8	4.6	0.88	0.08	94.1	0.02	10	0.01	58	38	2.34	150	2.35	−5.0	29.5
HLQ18	24.0	4.9	1.29	0.09	93.7	0.04	433	0.48	54	72	2.97	281	2.98	−2.6	0.5
FHQ17	12.7	15.8	3.66	0.25	80.2	0.08	718	0.28	62	145	2.81	568	2.81	−4.3	0.3
FHQ18	16.0	22.6	0.21	0.43	76.7	0.89	1845	0.43	53	359	3.18	1401	3.18	−2.5	0.1

(1) R_M/R_A is the observed $^3He/^4He$ ratio divided by the $^3He/^4He$ ratio in the air (1.39×10^{-6}, [42]). (2) $X = (^4He/^{20}Ne)_M/(^4He/^{20}Ne)_{Air} \times (\beta_{Ne}/\beta_{He})$, where β represents the Bunsen coefficients assuming a groundwater recharge temperature of 10°C ($\beta_{Ne}/\beta_{He} = 1.25$, [43]), $(^4He/^{20}Ne)_M$ is the measured ratio of samples, and $(^4He/^{20}Ne)_{Air}$ is the ratio of the air (0.32, [42]). (3) R_C/R_A is the air-corrected Helium isotope ratio by applying the following formula [44]: $R_C/R_A = ((R_M/R_A) \times X - 1)/(X - 1)$.

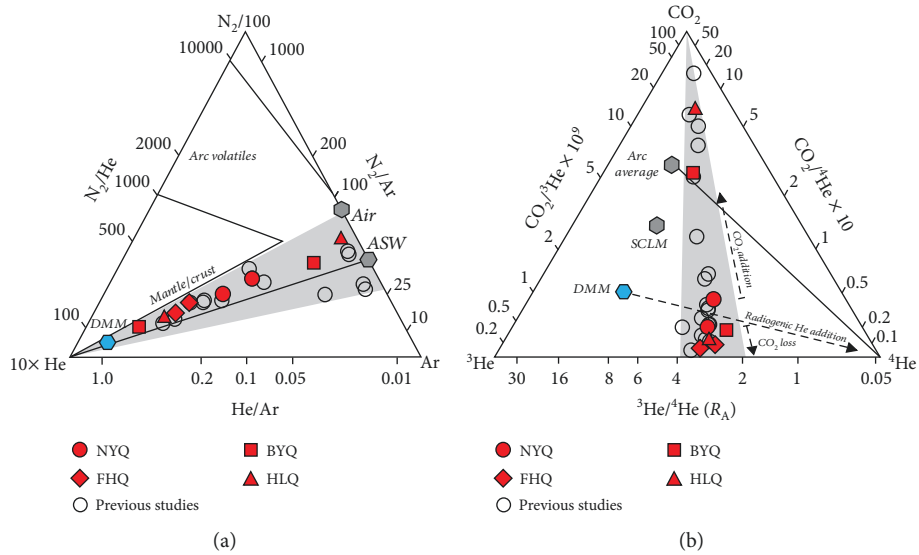

Figure 5: Triangle plot of N_2-He-Ar (a) and CO_2-^3He-^4He (b) for the cold spring gases in WMVF (modified from Giggenbach et al. [47]). Filled and open symbols represent, respectively, data in this study and published data in [18–22, 48]. The compiled data in previous studies are available in Supplementary Table S3. Abbreviations: NYQ: South spring; BYQ: North spring; FHQ: Fanhua spring; HLQ: Hualin spring; ASW: air-saturated water; Arc average: arc-related volatiles ($^3He/^4He = 5.4 \pm 1.9R_A$, [49]; $CO_2/^3He = (4.5\text{-}29) \times 10^9$, [46]); SCLM: subcontinental lithospheric mantle ($^3He/^4He = 6.1 \pm 0.9R_A$, [50]; $CO_2/^3He = 4 \times 10^9$, [51]); DMM: depleted MORB-source mantle ($^3He/^4He = 8 \pm 1R_A$, [52]; $CO_2/^3He = 1.5 \times 10^9$, [46]).

derived components related to the deep subduction of the Pacific plate, including the slab carbonate (CAR) and subducted organic sediments (ORS), are involved in the CO_2 inventory of the volatiles in the Changbaishan volcanic fields in NE China, which are similar to those from arc volcanism [46, 58–60]. The $CO_2/^3He$ ratio remains constant as the gas phase separates from molten basalt, because of the similar solubilities of CO_2 and He in melts [61]. Figure 6(a) shows the relationship between $CO_2/^3He$ ratios and $\delta^{13}C$ values of cold spring gases in the WMVF, whereas the $CO_2/^3He$ ratios of the dataset show marked disparity (Table 1; Figures 5(b) and 6).

Samples with $CO_2/^3He$ ratios lower than that of DMM are thought to result from the physical-chemical fractionation of CO_2 to He [46, 61] or variable $CO_2/^3He$ ratios of continental crustal contribution [62]. However, these samples with low $CO_2/^3He$ ratios in the WMVF basically have constant $^3He/^4He$ (R_A) ratios when compared to those within the three end members (Figures 7 and 6(b)), which eliminate the additional contribution from the crustal origin. Phase separation within the shallow aquifer can potentially fractionate elemental $CO_2/^3He$ ratios due to the greater solubility of CO_2 in the aqueous solution relative to that of the helium [43, 63], especially in low-temperature systems. For example, Sano et al. [64] suggested that a positive correlation between observed $CO_2/^3He$ ratios and temperatures of fumaroles and springs results from the differences in solubility. We thus suggest that the He-CO_2 fractionation in the cold shallow aquifer would act as the first-order controlling factor on these low $CO_2/^3He$ samples, including gas samples from the

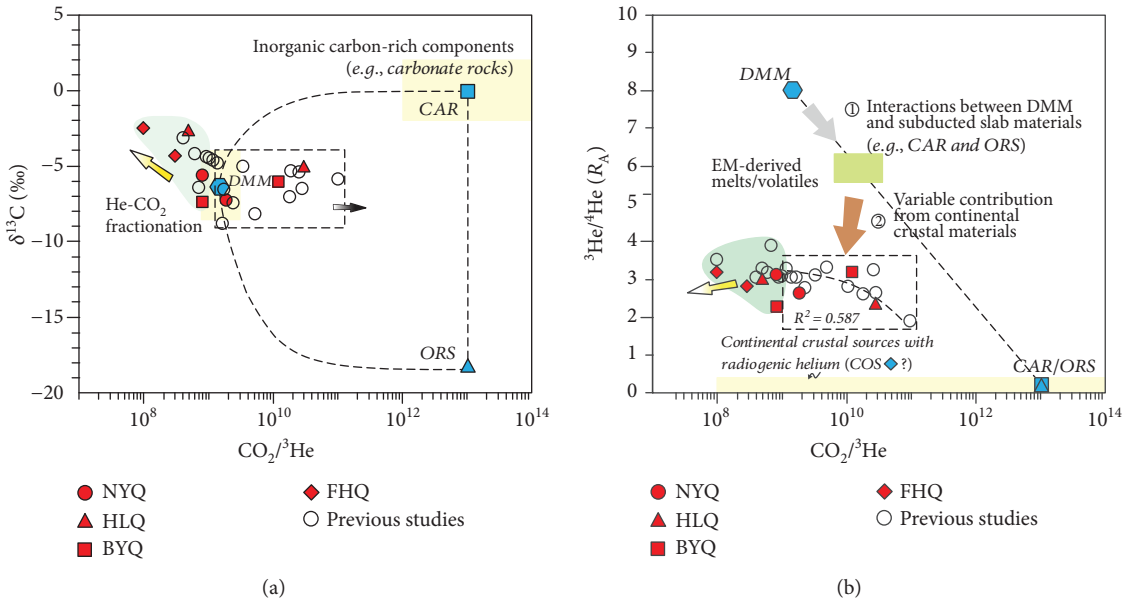

Figure 6: (a) $\delta^{13}C$ (‰) versus $CO_2/^3He$ ratios for cold spring gases from WMVF. The yellow arrow denotes the effects of He-CO_2 fractionation on the samples outside the mixing envelope. (b) $^3He/^4He$ (R_A) versus $CO_2/^3He$ ratios for cold spring gases from WMVF. Abbreviations and reference values for end members are as follows: CAR: carbonate rocks ($\delta^{13}C = 0 \pm 2$‰, [53]); ORS: organic sediments ($\delta^{13}C = -18.5$‰, [35]). The $^3He/^4He$ (R_A) ratios of CAR and ORS end members are assumed to be $0.02R_A$ [66] and the $CO_2/^3He$ values ranging from 10^{12} to 10^{14} [62]. The $CO_2/^3He$ ratios of DMM are ranging from 7.5×10^8 to 3×10^9, with an average of 1.5×10^9 [46]. The continental crustal source has a wide range of $CO_2/^3He$ ratios based on [62]. Data source and symbols are as in Figure 5.

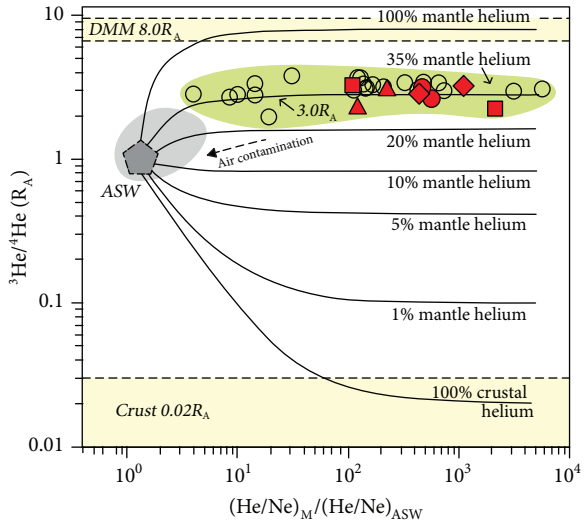

Figure 7: $^3He/^4He$ (R_A) versus $(He/Ne)_M/(He/Ne)_{ASW}$ for cold spring gases in WMVF. The calculated binary mixing curves between the air-saturated water (ASW) and crust-mantle mixtures with variable proportions of mantle helium (e.g., 100%, 35%, 20%, 10%, 5%, 1%, and 0%) are shown. Reference values for end members are as follows: ASW: $^3He/^4He = 0.987R_A$ [55], crust: $^3He/^4He = 0.02R_A$ [42] and $^4He/^{20}Ne = 3500$ [56], and DMM: $^4He/^{20}Ne = 5000$ [57]. Data source and symbols are as in Figure 5.

Fanhua spring, which are characterized by relatively high N_2 contents, low CO_2 contents, and low $CO_2/^3He$ ratios (Table 1; Figures 5 and 6). Considering this process, the original $CO_2/^3He$ ratios of gas samples may be higher than the observed values, as shown by the black arrow in Figure 6(a).

Samples within the mixing trajectories have contributions from DMM, ORS, and CAR end members (Figure 6(a)) [16, 46] and are used to calculate the proportion of their contributions to the total carbon inventory in the WMVF, as shown in Table 2. In this calculation, elemental fractionation and its effect on C-He isotope systematics are not considered. We took the average $\delta^{13}C$ (−18.5‰) of metamorphosed reduced carbon as that of the ORS end member when considering the potential fractionation during the subduction [16, 65]. If the contribution from continental crustal materials is not taken into account, an average proportion of subducted organic sediments (ORS) would be 24% (Table 2). The upper mantle and slab carbonate-derived carbon are the principal contributors to the carbon budget, with an average total contribution of 76% (Table 2), which is analogous to carbon inventories of worldwide arc magma-related volatiles [46, 58–60].

The diagram of $^3He/^4He$ (R_A) versus $CO_2/^3He$ ratios of volcanic or hydrothermal volatiles has provided important constraints on the origin of carbon [35, 61]. In Figure 6(b), the $^3He/^4He$ values of the studied samples within the mixing curves (Figure 6(a)) are negatively correlated with $CO_2/^3He$ ratios ($R^2 = 0.587$), further supporting the mixing between DMM or EM end member (both with high-R_A and low-$CO_2/^3He$ ratios) and subducted slab materials (CAR/ORS end member with low-R_A and high-$CO_2/^3He$ ratios) [67]. However, these samples are obviously located away from the above mixing line (Figure 5(b)), which shows a binary mixing trend between EM-derived volatiles

Table 2: Estimated carbon sources for the spring gas samples in WMVF.

Sample no.	Reference	$\delta^{13}C$ (‰)	$CO_2/^3He$ ($\times10^9$)	Carbon inventory			
				DMM	ORS	CAR	M+C
HLQ17	This study	−5.0	29.5	0.05	0.25	0.70	0.75
NYQ17	This study	−7.2	1.9	0.79	0.11	0.10	0.89
BYQ18	This study	−6.0	12.1	0.12	0.28	0.60	0.72
HL2	[21]	−5.3	18.8	0.08	0.26	0.66	0.74
FH2	[21]	−8.2	5.1	0.29	0.34	0.37	0.66
BY1	[21]	−6.5	28.5	0.05	0.33	0.61	0.66
NYQ	[18]	−5.1	27.0	0.06	0.26	0.69	0.76
WBQ	[18]	−5.8	97.6	0.02	0.30	0.68	0.70
DZT	[18]	−7.4	2.3	0.65	0.17	0.18	0.83
SG2	[20]	−6.6	1.7	0.88	0.05	0.07	0.95
			Average	0.30	0.24	0.46	0.76

and continental crustal materials with variable $CO_2/^3He$ ratios (Figure 6(b)) [62].

5.2. Origin and Evolution of the Volatiles in the WMVF

5.2.1. C-He Isotope Systematics and End-Member Parameters. In the C-He isotope systematics based on Van Soest et al. [59], $^3He/^4He$ ratios coupled with $\delta^{13}C_{CO2}$ values were applied to quantitatively constrain the evolution of volatiles (Figure 8). Following the deep subduction scenario, upper mantle (DMM), slab carbonate (CAR), and organic sediments (ORS) are involved in the origin of volatiles in the WMVF, which exhibited variable contribution of continental crustal components, including organic metasediments (COS) and crustal carbonate (CAR) during their ascending process (Figures 6(b) and 8). Reference values for associated parameters of end members used in the modelling calculation are listed in Table 3.

Helium concentration of the ORS end member was calculated based on the U-Th decay of the global subducting sediments (GLOSS with high SiO_2 content; see details in the Supplementary Material) with reservoir accumulation age of 2.2 Ga in the MTZ constrained by the lead isotope [13]. The COS end member was assumed to have a helium ratio equal to that of the bulk continental crust ($0.02R_A$, [66]). Considering the potential fractionation effects of the He-CO_2 system, the samples with lower $CO_2/^3He$ ratios than DMM (Figure 6) were not considered for further discussion when calculating the C-He isotope systematics (Figure 8). The results of the C-He isotope mixing calculations between different end members are listed in Supplementary Tables S5 and S6.

5.2.2. Nature of the Upper Mantle Enriched by CAR and ORS with respect to Melts beneath the WMVF. Melting of subducted carbonates (CAR) and/or organic sediments (ORS) would release volatiles, i.e., carbon dioxide [70], and generate hydrous-carbonated plumes (HCPs, [71]) and ORS-related silicate melts under the P-T conditions of the MTZ. Based on the C-He isotope systematics, binary mixing between carbonate and ambient depleted upper mantle was first considered to produce the carbonated peridotite (CP) (Figure 8). Interaction between CP and ORS-derived silicate melts would produce enriched upper mantle (EM), which is considered as the primary source of WMVF volatiles (Figures 6(b) and 8).

The best-fit mixing trajectory with $K = 1.71$ for mixing between ORS and CP was estimated based on an optimal $CO_2/^3He$ ratio of 10^{13} due to the lack of carbon contents in the assumed ORS end member, which lies above all the WMVF samples (Figure 8). K represents the ratio of He/C values between CP and ORS according to Van Soest et al. [59]. The carbon content (12618 ppm) in the ORS end member is obtained by calculation of the optimal K coefficient (1.71). The reasonable upper and lower limits for the CP-ORS mixing are marked by mixing trajectories with K values of 17.1 and 0.171, which yield $CO_2/^3He$ ratios of 10^{14} and 10^{12} [62], respectively.

As indicated by the C-He isotope systematics, EM-like $^3He/^4He$ and $\delta^{13}C$ ratios beneath WMVF are marked by $5.8R_A$ and −9.7‰ (5.5-$6.1R_A$, −10.3 to −9.1‰; Figures 8 and 9(b)), respectively. Such C-He isotopes indicate an involvement of 10% (in average; ranging from 8% to 13%) carbonate and 13% (in average; ranging from 11% to 15%) ORS-derived silicate melts in the depleted mantle source, along with the Nd-Mg isotope information from potassic basalts in the WMVF (Supplementary Material). Partial melting of the enriched upper mantle (EM) source would produce basaltic magmas and concomitant initial volatiles in the WMVF (Figures 8 and 9(b)).

5.2.3. Crustal Contribution of the Ascending EM-Derived Volatiles. Previous studies have shown that up to 6 km of sediments piled up and underwent significant heating subsidence associated with the early Cretaceous rifting in the Songliao basin [29, 31]. Buried materials consisted of carbonate sediments (CAR) and shallow organic metasediments (COS) [26, 27]. $CO_2/^3He$ ratios and C-He isotope values of the gas samples in the WMVF display obvious mixing evolution trends between the EM source and crustal components

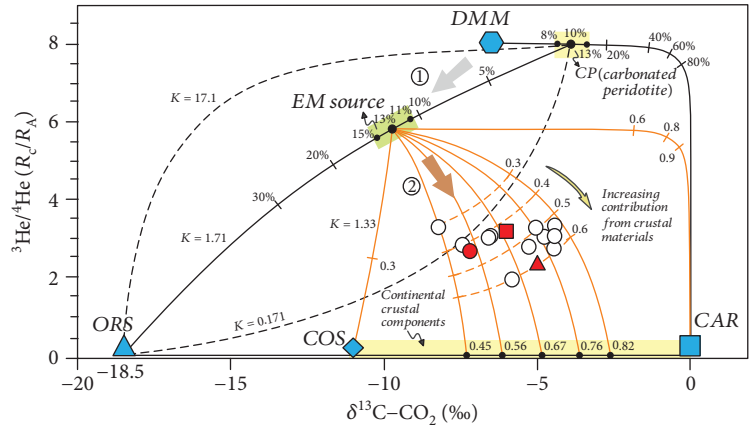

Figure 8: C-He isotope systematics showing a two-stage model for cold spring gases in WMVF. Stage 1: interactions between slab-derived melts (CAR and ORS) in MTZ and the depleted upper mantle (DMM); stage 2: the different proportions of crustal contribution (COS and CAR) during the ascending process of EM-derived volatiles. COS represents the continental organic metasediments.

Table 3: Reference values for associated parameters of DMM, CAR, ORS, and COS end members used in C-He isotope systematics.

End member	$\delta^{13}C_{CO2}$ (‰)	C contents (ppm)	$^3He/^4He$ (R_A)	He contents (ppm)	$CO_2/^3He$ ($\times10^9$)
DMM	−6.5[a]	1920[b]	8[a]	0.0288[b]	1.5[a]
CAR	0[c]	11400[d]	0.05[e]	0.00023[d]	1000-100000[f]
ORS	−18.5[g]	12618[j]	0.05[e]	0.0667[j]	1000-100000[f]
COS	−11[h]	Unknown	0.02[i]	Unknown	0.1-100000[f]

Data sources: [a][46], [b][37], [c][53], [d][59], [e][68], [f][62], [g][65], [h][69], and [i][66]. [j]Calculated based on U-Th decay.

which consists of different proportions of COS and CAR (Figures 6(b) and 8). As indicated by the C-He isotope mixing calculation, the proportion of crustal components (including COS and CAR) ranges from 30% to 60% of the overall carbon budget of the EM source-derived volatiles (Figure 8). In this binary mixing model, continental carbonate sediments (CAR) represent 45% to 82% of the crustal components (Figure 8).

5.3. Genetic Model of Deep CO_2 Emissions in the Songliao Continental Rift System. C-He isotope systematics provide constraint on the source region of volatiles collected at the surface in the WMVF. Following the Pacific oceanic crust deep subduction scenario, we proposed a two-stage model to explain the evolution process of cold spring gases in the WMVF. Firstly, the interactions between the depleted mantle and carbonated silicate melts (CAR and ORS) derived from a stagnant Pacific oceanic slab in the mantle transition zone (MTZ) produce an enriched upper mantle beneath WMVF (Figure 9(b)); secondly, EM-derived initial volatiles underwent different proportions of crustal input, including carbonates (CAR) and organic metasediments (COS) in the continental crust during their arising process (Figures 6(b), 8, and 9(a)). Deep-fed CO_2 is emitted into the atmosphere through spring bubbles and diffusive soil CO_2 emissions in the adjacent areas (Figures 9(a)).

This model provides an integrated constraint on the source region of cold spring gases (e.g., He and C isotopes) for further understanding the carbon cycling processes in the Songliao continental rift system beneath East Asia, which is supported by petrogenesis of potassic basalts erupted in 1721 AD [11–13] and evidence from seismic tomographic studies [14, 72]. The interactions between the MTZ-derived melts and the ambient upper mantle provide a plausible hypothesis to explain the lithospheric thinning, extensive continental rifting, Cenozoic intraplate basaltic volcanism, and magma-related degassing in East Asia (Figure 9(b)) [14, 16, 71].

6. Conclusions

Our modeling calculated results indicate that the average soil CO_2 flux in the Laoheishan volcano (11.8 g m^{-2} d^{-1}) is lower than that of the whole WMVF (18.7 g m^{-2} d^{-1}), which suggest weak degassing of the solidified underlying magma body beneath the Laoheishan volcano. On the basis of the C-He isotope mixing simulation results, we propose a two-stage model to constrain the provenance and evolution of volatiles in the WMVF. The first stage is concerned with the interactions between the depleted upper mantle (DMM) and the accumulated Pacific oceanic slab materials (CAR and ORS) in the MTZ and finally results in the formation of the enriched mantle source region (EM), which is considered as the primary source of cold spring gases in the WMVF. The second stage is related to the crustal contamination

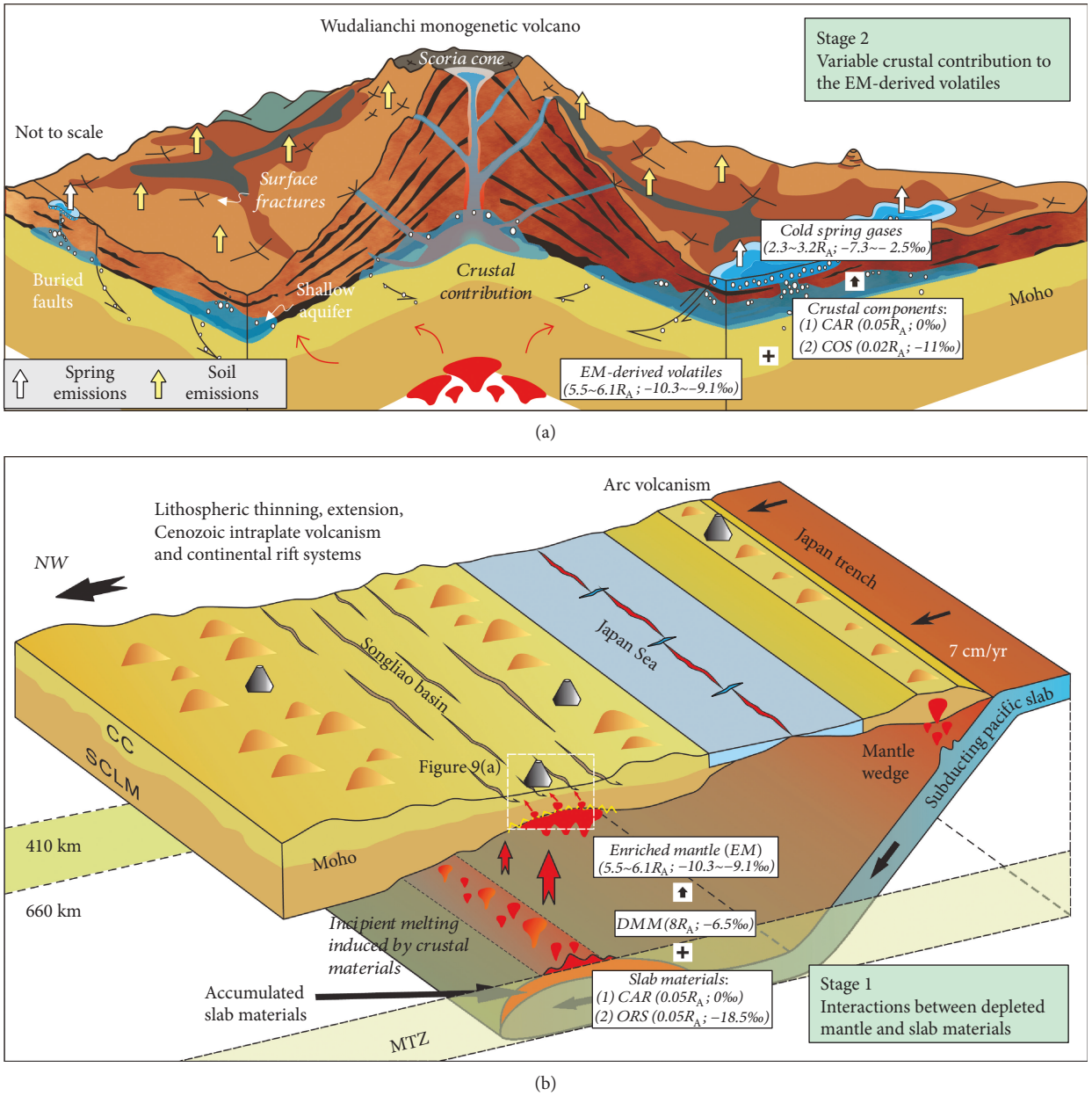

Figure 9: Genetic model of the cold spring gases in WMVF. (a) Crustal contribution to the EM-derived volatiles. (b) A schematic map shows the interactions between the depleted mantle and the slab materials in the MTZ. Abbreviations are as follows: MTZ: mantle transition zone; Moho: Mohorovičić discontinuity; SCLM: subcontinental lithospheric mantle; CC: continental crust.

(including continental organic metasediments and carbonates) when the CO_2-dominated gases rise to the surface.

Data Availability

The chemical and C-He isotope data of spring gases used to support the findings of this study are included within the article and the supplementary material.

Conflicts of Interest

The authors declare that they have no conflicts of interest.

Acknowledgments

This work was funded by the Strategic Priority Research Program of the Chinese Academy of Sciences (Grant No. XDB26000000), the Key Research Project of Frontier Sciences of the Chinese Academy of Sciences (Grant No. QYZDY-SSW-DQC030), and the National Science Foundation of China (Grant Nos. 41572321 and 41702361). We thank Drs. Lihong Zhang and Yutao Sun for interpreting the soil flux data. Drs. Liwu Li, Zhongping Li, Li Du, Lantian Xing, and Hengliang Gao are acknowledged for help in analyzing the samples.

Supplementary Materials

The Supplementary Materials file provides additional tables/figures and data mentioned in the revised manuscript, including (1) measured soil CO_2 fluxes of whole WMVF (Table S1) and SE slope of the Laoheishan volcanic cone (Table S2), (2) chemical and C-He isotopic compositions of spring gases in this and previous studies (Table S3), (3) detailed reference values for associated parameters (Table S4) and results (Table S5 and S6) in C-He isotope systematics, and (4) detailed reference values for associated parameters (Table S7) and results (Table S8 and Figure S1) in the Nd-Mg isotope coupling calculation. *(Supplementary Materials)*

References

[1] W. Hutchison, T. A. Mather, D. M. Pyle, J. Biggs, and G. Yirgu, "Structural controls on fluid pathways in an active rift system: a case study of the Aluto volcanic complex," *Geosphere*, vol. 11, no. 3, pp. 542–562, 2015.

[2] H. Lee, J. D. Muirhead, T. P. Fischer et al., "Massive and prolonged deep carbon emissions associated with continental rifting," *Nature Geoscience*, vol. 9, no. 2, pp. 145–149, 2016.

[3] J. D. Muirhead, S. A. Kattenhorn, H. Lee et al., "Evolution of upper crustal faulting assisted by magmatic volatile release during early–stage continental rift development in the East African Rift," *Geosphere*, vol. 12, no. 6, pp. 1670–1700, 2016.

[4] S. Brune, S. E. Williams, and R. D. Müller, "Potential links between continental rifting, CO_2 degassing and climate change through time," *Nature Geoscience*, vol. 10, no. 12, pp. 941–946, 2017.

[5] S. F. Foley and T. P. Fischer, "An essential role for continental rifts and lithosphere in the deep carbon cycle," *Nature Geoscience*, vol. 10, no. 12, pp. 897–902, 2017.

[6] G. Tamburello, S. Pondrelli, G. Chiodini, and D. Rouwet, "Global–scale control of extensional tectonics on CO_2 earth degassing," *Nature Communications*, vol. 9, no. 1, article 4608, 2018.

[7] T. O. Rooney, W. R. Nelson, L. Dosso, T. Furman, and B. Hanan, "The role of continental lithosphere metasomes in the production of HIMU–like magmatism on the Northeast African and Arabian plates," *Geology*, vol. 42, no. 5, pp. 419–422, 2014.

[8] N. H. Sleep, "Stagnant lid convection and carbonate metasomatism of the deep continental lithosphere," *Geochemistry Geophysics Geosystems*, vol. 10, no. 11, article Q11010, 2009.

[9] W. Hutchison, T. A. Mather, D. M. Pyle et al., "The evolution of magma during continental rifting: new constraints from the isotopic and trace element signatures of silicic magmas from Ethiopian volcanoes," *Earth and Planetary Science Letters*, vol. 489, pp. 203–218, 2018.

[10] J. Liu, J. Han, and W. S. Fyfe, "Cenozoic episodic volcanism and continental rifting in Northeast China and possible link to Japan Sea development as revealed from K-Ar geochronology," *Tectonophysics*, vol. 339, no. 3–4, pp. 385–401, 2001.

[11] T. Kuritani, J. I. Kimura, E. Ohtani, H. Miyamoto, and K. Furuyama, "Transition zone origin of potassic basalts from Wudalianchi volcano, Northeast China," *Lithos*, vol. 156-159, pp. 1–12, 2013.

[12] H. C. Tian, W. Yang, S. G. Li, S. Ke, and Z. Y. Chu, "Origin of low δ^{26}Mg basalts with EM-I component: evidence for interaction between enriched lithosphere and carbonated asthenosphere," *Geochimica et Cosmochimica Acta*, vol. 188, pp. 93–105, 2016.

[13] X. J. Wang, L. H. Chen, A. W. Hofmann et al., "Mantle transition zone-derived EM1 component beneath NE China: geochemical evidence from Cenozoic potassic basalts," *Earth and Planetary Science Letters*, vol. 465, pp. 16–28, 2017.

[14] G. C. Richard and H. Iwamori, "Stagnant slab, wet plumes and Cenozoic volcanism in East Asia," *Physics of the Earth and Planetary Interiors*, vol. 183, no. 1-2, pp. 280–287, 2010.

[15] W. Wei, J. O. S. Hammond, D. Zhao, J. Xu, Q. Liu, and Y. Gu, "Seismic evidence for a mantle transition zone origin of the Wudalianchi and Halaha volcanoes in Northeast China," *Geochemistry, Geophysics, Geosystems*, vol. 20, no. 1, pp. 398–416, 2019.

[16] M. Zhang, Z. Guo, Y. Sano, Z. Cheng, and L. Zhang, "Stagnant subducted Pacific slab-derived CO_2 emissions: insights into magma degassing at Changbaishan volcano, NE China," *Journal of Asian Earth Sciences*, vol. 106, pp. 49–63, 2015.

[17] M. Zhang, Z. Guo, J. Liu et al., "The intraplate Changbaishan volcanic field (China/North Korea): a review on eruptive history, magma genesis, geodynamic significance, recent dynamics and potential hazards," *Earth-Science Reviews*, vol. 187, pp. 19–52, 2018.

[18] J. Du, S. Li, Y. Zhao, J. Ren, R. Sun, and H. Duanmu, "Geochemical Characteristics of Gases from the Wudalianchi Volcanic Area, Northeastern China," *Acta Geologica Sinica - English Edition*, vol. 73, no. 2, pp. 225–229, 1999.

[19] Z. Shangguan, C. Zhao, and L. Gao, "Carbon isotopic compositions of the methane derived from magma at the active volcanic regions in China," *Acta Petrologica Sinica*, vol. 22, pp. 1458–1464, 2006.

[20] Z. Shangguan and C. Wu, "Geochemical features of magmatic gases in the regions of dormant volcanos in China," *Acta Petrologica Sinica*, vol. 24, pp. 2638–2646, 2008.

[21] X. Mao, Y. Wang, O. V. Chudaev, and X. Wang, "Geochemical evidence of gas sources of CO_2-rich cold springs from Wudalianchi, Northeast China," *Journal of Earth Science*, vol. 20, no. 6, pp. 959–970, 2009.

[22] S. Xu, G. Zheng, S. Nakai, H. Wakita, X. Wang, and Z. Guo, "Hydrothermal He and CO_2 at Wudalianchi intra-plate volcano, NE China," *Journal of Asian Earth Sciences*, vol. 62, pp. 526–530, 2013.

[23] Y. W. Zhao, N. Li, Q. C. Fan, H. Zou, and Y. G. Xu, "Two episodes of volcanism in the Wudalianchi volcanic belt, NE China: evidence for tectonic controls on volcanic activities," *Journal of Volcanology and Geothermal Research*, vol. 285, pp. 170–179, 2014.

[24] L. Xiao and C. Wang, "Geologic features of Wudalianchi volcanic field, Northeastern China: implications for Martian volcanology," *Planetary and Space Science*, vol. 57, no. 5–6, pp. 685–698, 2009.

[25] L. Zhang, X. Zhou, J. Ying et al., "Geochemistry and Sr-Nd-Pb-Hf isotopes of Early Cretaceous basalts from the Great Xinggan Range, NE China: implications for their origin and mantle source characteristics," *Chemical Geology*, vol. 256, no. 1–2, pp. 12–23, 2008.

[26] C. Huang, G. J. Retallack, C. Wang, and Q. Huang, "Paleoatmospheric pCO_2 fluctuations across the Cretaceous–Tertiary boundary recorded from paleosol carbonates in NE China," *Palaeogeography Palaeoclimatology Palaeoecology*, vol. 385, pp. 95–105, 2013.

[27] Y. Gao, D. E. Ibarra, C. Wang et al., "Midlatitude terrestrial climate of East Asia linked to global climate in the late cretaceous," *Geology*, vol. 43, no. 4, pp. 287–290, 2015.

[28] T. L. Barry and R. W. Kent, "Cenozoic magmatism in Mongolia and the origin of central and east Asian basalts," in *Mantle Dynamics and Plate Interactions in East Asia Geodynamics*, M. F. J. Flower, S. L. Chung, C. H. Lo, and T. Y. Lee, Eds., pp. 347–364, American Geophysical Union, Washington, D. C., 1998.

[29] Y. Wang and H. Chen, "Tectonic controls on the Pleistocene-Holocene Wudalianchi volcanic field (Northeastern China)," *Journal of Asian Earth Sciences*, vol. 24, no. 4, pp. 419–431, 2005.

[30] J. Ren, K. Tamaki, S. Li, and Z. Junxia, "Late Mesozoic and Cenozoic rifting and its dynamic setting in Eastern China and adjacent areas," *Tectonophysics*, vol. 344, no. 3-4, pp. 175–205, 2002.

[31] R. Zhang, Q. Wu, L. Sun, J. He, and Z. Gao, "Crustal and lithospheric structure of Northeast China from S-wave receiver functions," *Earth and Planetary Science Letters*, vol. 401, pp. 196–205, 2014.

[32] H. U. Schmincke, *Volcanism*, Springer, Berlin, Heidelberg, 2004.

[33] Z. Li, S. Ni, B. Zhang et al., "Shallow magma chamber under the Wudalianchi volcanic field unveiled by seismic imaging with dense array," *Geophysical Research Letters*, vol. 43, no. 10, pp. 4954–4961, 2016.

[34] G. Chiodini, R. Cioni, M. Guidi, B. Raco, and L. Marini, "Soil CO_2 flux measurements in volcanic and geothermal areas," *Applied Geochemistry*, vol. 13, no. 5, pp. 543–552, 1998.

[35] M. Zhang, Z. Guo, Y. Sano et al., "Magma-derived CO_2 emissions in the Tengchong volcanic field, SE Tibet: implications for deep carbon cycle at intra-continent subduction zone," *Journal of Asian Earth Sciences*, vol. 127, pp. 76–90, 2016.

[36] M. Luo, H. Huang, P. Zhang, Q. Wu, and D. Chen, "Origins of gas discharging from the Qiangtang Basin in the northern Qinghai–Tibet Plateau, China: evidence from gas compositions, helium, and carbon isotopes," *Journal of Geochemical Exploration*, vol. 146, pp. 119–126, 2014.

[37] L. Zhang, Z. Guo, Y. Sano et al., "Flux and genesis of CO_2 degassing from volcanic-geothermal fields of Gulu-Yadong rift in the Lhasa terrane, South Tibet: Constraints on characteristics of deep carbon cycle in the India-Asia continent subduction zone," *Journal of Asian Earth Sciences*, vol. 149, pp. 110–123, 2017.

[38] A. J. Sinclair, "Selection of threshold values in geochemical data using probability graphs," *Journal of Geochemical Exploration*, vol. 3, no. 2, pp. 129–149, 1974.

[39] G. Chiodini, S. Caliro, C. Cardellini, R. Avino, D. Granieri, and A. Schmidt, "Carbon isotopic composition of soil CO_2 efflux, a powerful method to discriminate different sources feeding soil CO_2 degassing in volcanic-hydrothermal areas," *Earth and Planetary Science Letters*, vol. 274, no. 3-4, pp. 372–379, 2008.

[40] A. Caracausi, M. Paternoster, and P. M. Nuccio, "Mantle CO_2 degassing at Mt. Vulture volcano (Italy): relationship between CO_2 outgassing of volcanoes and the time of their last eruption," *Earth and Planetary Science Letters*, vol. 411, pp. 268–280, 2015.

[41] Y. Zhan, G. Zhao, J. Wang, Q. Xiao, J. Tang, and I. I. Rokityansky, "Crustal electric conductivity structure for Wudalianchi volcanic cluster in the Heilongjiang province, China," *Acta Petrologica Sinica*, vol. 22, no. 6, pp. 1495–1502, 2006.

[42] M. Ozima and F. A. Podosek, *Noble Gas Geochemistry*, Cambridge University Press, London, 1983.

[43] R. F. Weiss, "Solubility of helium and neon in water and seawater," *Journal of Chemical & Engineering Data*, vol. 16, no. 2, pp. 235–241, 1971.

[44] D. R. Hilton, "The helium and carbon isotope systematics of a continental geothermal system: results from monitoring studies at Long Valley caldera (California, U.S.A.)," *Chemical Geology*, vol. 127, no. 4, pp. 269–295, 1996.

[45] T. H. E. Heaton and J. C. Vogel, "Gas concentrations and ages of groundwaters in Beaufort group sediments, South Africa," *Water South Africa*, vol. 5, no. 4, pp. 160–170, 1979.

[46] Y. Sano and B. Marty, "Origin of carbon in fumarolic gas from island arcs," *Chemical Geology*, vol. 119, no. 1–4, pp. 265–274, 1995.

[47] W. F. Giggenbach, Y. Sano, and H. Wakita, "Isotopic composition of helium, and CO_2 and CH_4 contents in gases produced along the New Zealand part of a convergent plate boundary," *Geochimica et Cosmochimica Acta*, vol. 57, no. 14, pp. 3427–3455, 1993.

[48] R. Sun, Z. Pan, Y. Pan, and S. Yang, "Escaping gas He isotope assaying of the outcorop spring and study on the volcanic activity in Wudalianchi area," *Seismological Research of Northeast China*, vol. 24, no. 1, pp. 61–65, 2008.

[49] D. R. Hilton, T. P. Fischer, and B. Marty, "Noble gases and volatile recycling at subduction zones," *Reviews in Mineralogy and Geochemistry*, vol. 47, no. 1, pp. 319–370, 2002.

[50] C. Gautheron and M. Moreira, "Helium signature of the subcontinental lithospheric mantle," *Earth and Planetary Science Letters*, vol. 199, no. 1–2, pp. 39–47, 2002.

[51] D. Hahm, D. R. Hilton, M. Cho, H. Wei, and K. R. Kim, "Geothermal He and CO_2 variations at Changbaishan intra–plate volcano (NE China) and the nature of the sub-continental lithospheric mantle," *Geophysical Research Letters*, vol. 35, no. 22, article L22304, 2008.

[52] D. R. Hilton and H. Craig, "A helium isotope transect along the Indonesian archipelago," *Nature*, vol. 342, no. 6252, pp. 906–908, 1989.

[53] J. Hoefs, *Stable Isotope Geochemistry*, Springer, Berlin Heidelberg, 2009.

[54] J. M. de Moor, T. P. Fischer, Z. D. Sharp et al., "Gas chemistry and nitrogen isotope compositions of cold mantle gases from Rungwe Volcanic Province, southern Tanzania," *Chemical Geology*, vol. 339, pp. 30–42, 2013.

[55] S. L. Klemperer, B. M. Kennedy, S. R. Sastry, Y. Makovsky, T. Harinarayana, and M. L. Leech, "Mantle fluids in the Karakoram fault: helium isotope evidence," *Earth and Planetary Science Letters*, vol. 366, pp. 59–70, 2013.

[56] P. H. Barry, D. R. Hilton, T. P. Fischer, J. M. de Moor, F. Mangasini, and C. Ramirez, "Helium and carbon isotope systematics of cold "mazuku" CO_2 vents and hydrothermal gases and fluids from Rungwe Volcanic Province, southern Tanzania," *Chemical Geology*, vol. 339, pp. 141–156, 2013.

[57] Y. Sano, T. Tominaga, Y. Nakamura, and H. Wakita, "$^3He/^4He$ ratios of methane–rich natural gases in Japan," *Geochemical Journal*, vol. 16, no. 5, pp. 237–245, 1982.

[58] Y. Sano and S. N. Williams, "Fluxes of mantle and subducted carbon along convergent plate boundaries," *Geophysical Research Letters*, vol. 23, no. 20, pp. 2749–2752, 1996.

[59] M. C. Van Soest, D. R. Hilton, and R. Kreulen, "Tracing crustal and slab contributions to arc magmatism in the Lesser Antilles island arc using helium and carbon relationships in geothermal fluids," *Geochimica et Cosmochimica Acta*, vol. 62, no. 19–20, pp. 3323–3335, 1998.

[60] A. M. Shaw, D. R. Hilton, T. P. Fischer, J. A. Walker, and G. E. Alvarado, "Contrasting He–C relationships in Nicaragua and Costa Rica: insights into C cycling through subduction zones," *Earth and Planetary Science Letters*, vol. 214, no. 3-4, pp. 499–513, 2003.

[61] B. Marty and A. Jambon, "$C/^3He$ in volatile fluxes from the solid earth: implications for carbon geodynamics," *Earth and Planetary Science Letters*, vol. 83, no. 1–4, pp. 16–26, 1987.

[62] R. K. O'Nions and E. R. Oxburgh, "Helium, volatile fluxes and the development of continental crust," *Earth and Planetary Science Letters*, vol. 90, no. 3, pp. 331–347, 1988.

[63] H. Stephen and T. Stephen, *Solubilities of inorganic and organic compounds, binary systems (1), part 1*, Pergamon press, New York, 1963.

[64] Y. Sano, J. I. Hirabayashi, T. Oba, and T. Gamo, "Carbon and helium isotopic ratios at Kusatsu-Shirane volcano, Japan," *Applied Geochemistry*, vol. 9, no. 4, pp. 371–377, 1994.

[65] J. Cook-Kollars, G. E. Bebout, N. C. Collins, S. Angiboust, and P. Agard, "Subduction zone metamorphic pathway for deep carbon cycling: I. Evidence from HP/UHP metasedimentary rocks, Italian Alps," *Chemical Geology*, vol. 386, pp. 31–48, 2014.

[66] J. E. Lupton, "Terrestrial inert gases isotope tracer studies and clues to primordial components in the mantle," *Annual Review of Earth and Planetary Sciences*, vol. 11, no. 1, pp. 371–414, 1983.

[67] R. J. Poreda, A. W. A. Jeffrey, I. R. Kaplan, and H. Craig, "Magmatic helium in subduction-zone natural gases," *Chemical Geology*, vol. 71, no. 1–3, pp. 199–210, 1988.

[68] J. N. Andrews, "The isotopic composition of radiogenic helium and its use to study groundwater movement in confined aquifers," *Chemical Geology*, vol. 49, no. 1–3, pp. 339–351, 1985.

[69] J. Hoefs and M. Frey, "The isotopic composition of carbonaceous matter in a metamorphic profile from the Swiss Alps," *Geochimica et Cosmochimica Acta*, vol. 40, no. 8, pp. 945–951, 1976.

[70] R. Dasgupta, M. M. Hirschmann, and A. C. Withers, "Deep global cycling of carbon constrained by the solidus of anhydrous, carbonated eclogite under upper mantle conditions," *Earth and Planetary Science Letters*, vol. 227, no. 1-2, pp. 73–85, 2004.

[71] I. Safonova, S. Maruyama, and K. Litasov, "Generation of hydrous-carbonated plumes in the mantle transition zone linked to tectonic erosion and subduction," *Tectonophysics*, vol. 662, pp. 454–471, 2015.

[72] D. Zhao, S. Maruyama, and S. Omori, "Mantle dynamics of Western Pacific and East Asia: insight from seismic tomography and mineral physics," *Gondwana Research*, vol. 11, no. 1–2, pp. 120–131, 2007.